Sustainable Energy & Fuels, 2020, DOI: 10.1039/DOSE00623H

Highly efficient formic acid and carbon dioxide electro-reduction to alcohols on indium oxide electrodes

Kayode Adesina Adegoke,[1] Shankara Gayathri Radhakrishnan,[1] Clarissa L. Gray,[1] Barbara Sowa,[1‡] Claudia Morais,[2] Paul Rayess,[2] Egmont, R. Rohwer, Clément Comminges,[2]* K. Boniface Kokoh,[2] Emil Roduner[1,3]*

Formic acid is often assumed to be the first intermediate of carbon dioxide reduction to alcohols or hydrocarbons. Here we use co-electrolysis of water and aqueous formic acid in a PEM electrolysis cell with Nafion® as a polymer electrolyte, a standard TaC-supported IrO_2 water-splitting catalyst at the anode, and nanosize In_2O_3 with a small amount of added polytetrafluoroethylene (PTFE) as the cathode. This results in a mixture of methanol, ethanol and iso-propanol with a maximum combined Faraday efficiency of 82.5%. In the absence of diffusion limitation, a current density up to 70 mA cm^{-2} is reached, and the space-time-yield compares well with results from heterogeneous In_2O_3 catalysis. Reduction works more efficiently with dissolved CO_2 than with formic acid, but the product distribution is different, suggesting that CO_2 reduction occurs primarily via a competing pathway that bypasses formic acid as an intermediate.

Introduction

A hot topic of recent times, the interest in recycling carbon dioxide to renewable liquid fuels or other valuable chemicals has rocketed since the adoption of the Paris Agreement on Climate Change. This is due to the EU ruling that from 2020 a considerable fraction of renewable fuel of non-biological origin has to be added to gasoline [1] and the commitment of large air carriers like United Airline to go 50% carbon neutral by 2050.

Heterogeneous catalysis and electrocatalysis are competing methods for recycling carbon dioxide to value chemicals. Since renewable energies are available mostly in the form of electricity, electrocatalysis is the obvious first choice with the advantage that strongly endothermic reactions are also accessible at room temperature since the reaction free energy is provided electrically instead of thermally. This allows the use of water directly as the source of hydrogen. At present, electrochemical reactions of large-scale industrial importance involve double electron transfer (fuel cell, water and chloralkali electrolysis) or three electrons per Al^{3+} in aluminium production from bauxite, but it appears to be a particular challenge to synthesise C_2 and higher carbon compounds by multi-electron transfer from CO_2. Given industrial applications, it is essential to design processes which can be conducted with high product yields and energy efficiency at low cost, which implies high current densities at low overpotentials.

Until recently, copper was the only metal electrode where products of CO_2 reduction with more than a single carbon were obtained, although at low current densities and Faraday efficiencies (FE).[2] Since then, ethylene, ethanol and n-propanol were reported with up to 50% Faraday efficiencies and current densities up to 10 mA·cm^{-2} using Cu nanoparticles.[3] Cu nanoparticles supported on N-doped graphene showed 84% selectivity and 63% FE to ethanol formation, though still at low current densities.[4] Novel electrocatalysts such as nickel phosphides producing methylglyoxal and 2,3-furandiol show very high Faraday and energy efficiencies and therefore look promising.[5]

100% methanol selectivity from CO_2 and hydrogen was achieved using zirconia-supported indium oxide as a heterogeneous catalyst at a temperature of 300 °C and a pressure of 5.0 MPa, giving a threefold space-time-yield and a sizable increase in stability compared to the previous benchmark system, Cu-ZnO-Al_2O_3.[6] Methanol formation with its selectivity exceeding 80% was reported for PdIn intermetallic nanoparticles.[7,8]

[1] *Department of Chemistry, University of Pretoria, Pretoria 0002, South Africa*
[2] Université de Poitiers, 4 rue Michel Brunet, IC2MP UMR-CNRS 7285, TSA 51106, 86073 Poitiers cedex 9, France
[3] Institute of Physical Chemistry, University of Stuttgart, Pfaffenwaldring 55, D-70569 Stuttgart, Germany

‡ Present address: Laboratory for Chemical Technology, Ghent University, Technologiepark 125, B-9052 Ghent, Belgium

Electronic Supplementary Information (ESI) available: [Methods; In-situ spectro-electrochemical analysis of intermediates Ex-situ GC product analysis and efficiency aspects; Bixbyite structure of crystalline In_2O_3]. See DOI: 10.1039/x0xx00000x

Herein, we investigate whether In_2O_3 can also act as an electrocatalyst. This material is a transparent semiconductor with a bandgap of 2.7 eV.[9] Electrical conductivity is commonly achieved by doping with tin, forming the popular transparent indium tin oxide. Nitrogen-doping leads to excellent electrocatalytic activity for use in dye-sensitized solar cells,[10] but doping may not be necessary for nanomaterials since defects are generally abundant in oxides, in particular near surfaces. Anodized indium metal electrodes were shown to produce formate from CO_2.[11] The reduction activity was enhanced over indium-based nanoparticles.[12] Formate production at current densities up to 30 mA·cm^{-2} at Faraday efficiencies up to 80% were reported for in-situ grown indium-based catalysts.[13] Dominant formate with CO and methanol production in competition with H_2 was found with V-doped In_2O_3 nanocrystals. [14] In-situ prepared In_2O_3 reduced CO_2 to CO at low overpotentials of ca. 1.0 V against Ag/AgCl.[15]

The productivity of electrochemical conversion is often limited by gas diffusion through a liquid electrolyte to or from the surface of the catalyst. A catalyst-ionomer bulk heterojunction comprising a metal and an ionomer layer with hydrophobic and hydrophilic functionalities that decouples gas, ion and electron transport up to the micrometer scale allowed multicarbon product formation from CO_2 electrolysis at activities > 1 A·cm^{-2}.[16]

The aim of the present work is the development of a simple electrochemical system for future industrial-scale synthesis of renewable liquid solar fuels from CO_2. The focus is on co-electrolysis of water and formic acid, assuming that it is the first intermediate of CO_2 reduction, the initial experiments were also conducted with aqueous CO_2 solutions. The cathode catalyst is easy-to-prepare plain nanocrystalline In_2O_3 with added Nafion® and polytetrafluoroethylene to enhance diffusive access of the reactants to the catalyst and facilitate removal of the products. Minimization of the Ohmic resistance is essential to limit losses and requires short diffusive transport distances between the cathode and anode. This suggests the use of a polymer electrolyte membrane setup, which avoids the build-up of diffusion gradients in the catholyte. Furthermore, the electrode reaction should permit high current densities with high selectivity to liquid fuels and low yield of competing gas-phase products such as H_2, CO, and CH_4.

Experimental methods

Two types of electrochemical cells are used, firstly a polymer electrolyte membrane (PEM) water electrolysis cell with a standard TaC-supported IrO_2 water splitting anode catalyst on Nafion®. The cathode catalyst is the focus of the present work. It consists of In_2O_3 coated on carbon paper that acts as gas diffusion layer, and titanium mesh as current collector. Electrochemical analytical tools include cyclic voltammetry (CV), linear sweep voltammetry (LSV) and chronoamperometry (CA). The products from stationary electrolysis experiments are collected from the catholyte for GC analysis. Secondly, an infrared spectroelectrochemical cell with In_2O_3 supported on a glassy carbon electrode permits *in situ* analysis of the change of reactant concentrations and ideally the identification of intermediates (Figure 1).

Further experimental details are reported in the electronic supplementary information (ESI).

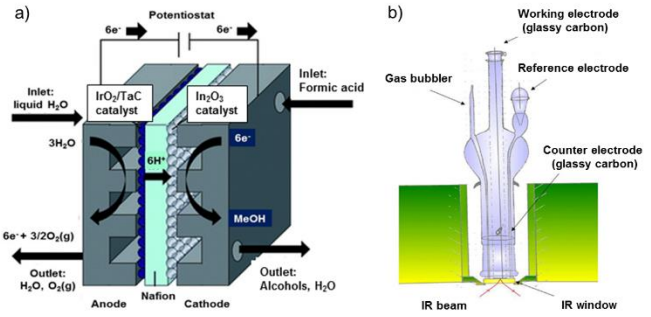

Figure 1: a) Electrolyzer cell (an inverse direct-methanol fuel cell), b) infrared spectroelectrochemical cell. (Two-column figure)

Results and discussion

Insight from cyclic voltammetry

The cyclic voltammogram of the In_2O_3 electrode (Figure 2a) in Na_2SO_4 electrolyte displays the characteristic redox couple In_2O_3/In, both under N_2 (blue trace) and CO_2 (red trace) atmospheres with a cathodic peak (c_1) at −0.50 V *vs*. the reversible hydrogen electrode (RHE) and an anodic peak (a_1) at −0.10 V *vs.* RHE. It was demonstrated recently that In_2O_3 nanoparticles can be reduced electrochemically to In^0-In_2O_3 composites which convert aqueous CO_2 nearly quantitatively at low potentials to CO. The reaction products of CO_2 can be tuned by the oxidation state of the In-based catalyst.[15] In the presence of formic acid (FA), the cyclic voltammogram is significantly modified as shown in Figure 2b. The c_1 wave related to In^{III} reduction is cathodically shifted to a value of −0.816 V *vs*. RHE, showing that In_2O_3 reduction is more difficult in the presence of FA. This can be explained by strong adsorption of FA on the oxide. A second reduction peak (c_2) is observed at −1.29 V *vs*. RHE. At a more cathodic potential, the hydrogen evolution reaction (HER) becomes dominant (c_3 wave). On the anodic scan, a sharp oxidation peak (a_1) is observed at −0.242 V *vs*. RHE. Its full width at half maximum of 67 mV is characteristic of a bielectronic transfer occurring on an immobilized species with a transfer coefficient α = 0.5 and a low rate constant.[17] Considering the stable oxidation state of In above the a_1 peak is +3, and the a_1 oxidation is bielectronic, this means that a In^I species is oxidized during the anodic scan. Integration of the a_1 and c_1 peaks shows that the coulometry of the c_1 peak is twice that of a_1, suggesting that 4 electrons are transferred on the c_1 reduction peak. As the reduction of In^{III} to In^0 implies the transfer of only 3 electrons, another electrochemical process must be involved. It can be envisioned that a proton undergoes a one-electron reduction to form an activated adsorbed hydrogen in the form In-H^*_{ads}. This reaction occurs as soon as In^0 is formed, as recently suggested for gas phase catalytic hydrogenation of CO_2 on

indium oxide [18] where a surface hydride was observed. This surface adsorbed hydrogen In-H^*_{ads}. can then reduce FA stepwise to alcohols by transferring 2 electrons, thus producing In^I as a transient species that is readily reduced to In^0 at the c_1 potential, or reoxidized to In^{III} at the a_1 potential as a bielectronic transfer.

Recently, Kim et al. [14] produced methanol from CO_2 on V-doped In_2O_3 with FE = 15.8% at –0.83 V *vs.* RHE, which coincides with the c_1 peak in Figure 2b.

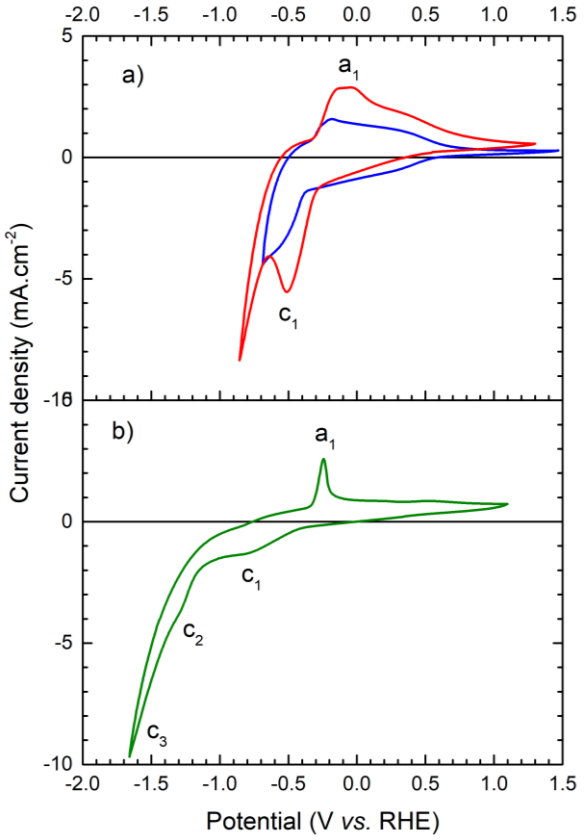

Figure 2: Cyclic voltammogram of In_2O_3 with 0.15 wt% PTFE deposited onto a glassy carbon electrode in 0.10 mol·L^{-1} aqueous Na_2SO_4 solution, a) saturated with N_2 (blue, pH 8.08), CO_2 (red, pH 5.24), and b) 4.3 mol·L^{-1} aqueous FA solution in 0.10 mol·L^{-1} Na_2SO_4 saturated with N_2 (green, pH 1.8). Scan rate: 50 mV·s^{-1}.

In situ IR spectroelectrochemical analysis of intermediates and mechanisms

a) Overview of electrochemical behavior from LSV

The LSV curves of a PTFE-free In_2O_3 electrode in 0.1 mol·L^{-1} Na_2SO_4 under N_2, CO_2 and in 4.3 mol·L^{-1} FA are compared in Figure 3a with the cathode potential given *vs*. RHE. A relatively small current density is observed in the presence of N_2 (black trace). A moderate reductive current is observed when the electrolyte is saturated with CO_2 (red trace). With FA, the current is reductive at negative potentials, and oxidative above this value (blue trace). This blue curve in Figure 3a clearly shows two oxidation peaks; a_1 and a_2, which according to Figure 3b are both accompanied by the disappearance of FA (see below). They relate to FA that may be oxidized at different surface sites on the catalyst, and to the catalyst oxidation itself as shown in Figure 2.

It is instructive to compare the current densities in Figure 3a since they are directly related to product formation. At a potential of –0.45 V *vs.* RHE, the CO_2-saturated solution provides –0.46 mA·cm^{-2}, whereas the FA solution yields –2.16 mA·cm^{-2}. The solubility of CO_2 in water amounts to ca. 0.034 mol·L^{-1} at 1 bar and room temperature, which is a factor of 126 less than the concentration of FA, while the current density is only a factor of 4.7 less. This suggests that aqueous CO_2 reacts much more efficiently on In_2O_3 than FA, although at a somewhat different pH. Hydrogen evolution from water splitting is often an undesirable competing reaction to CO_2 or FA reduction. In the absence of CO_2 and FA (black curve in Figure 3a) it is the only option, but the current density remains low in the given potential window, which is promising in view of high product yields other than H_2, although this may change at more negative potentials.

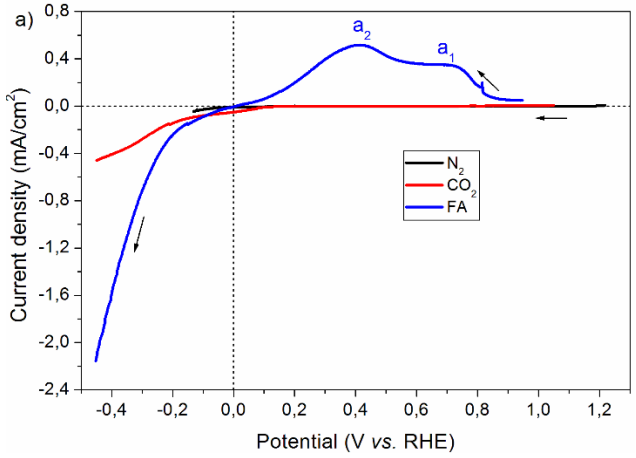

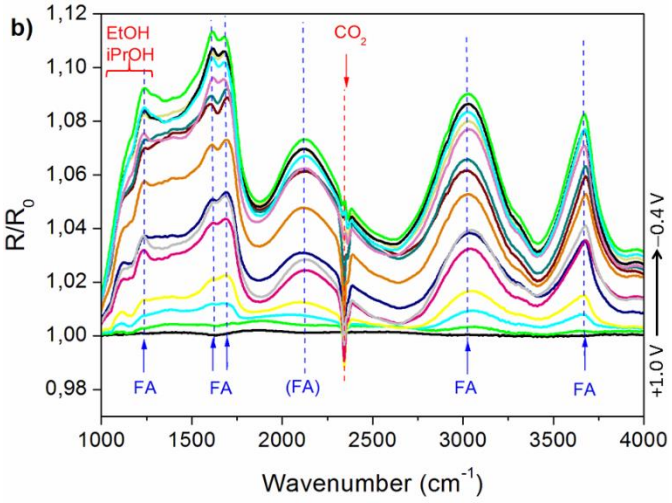

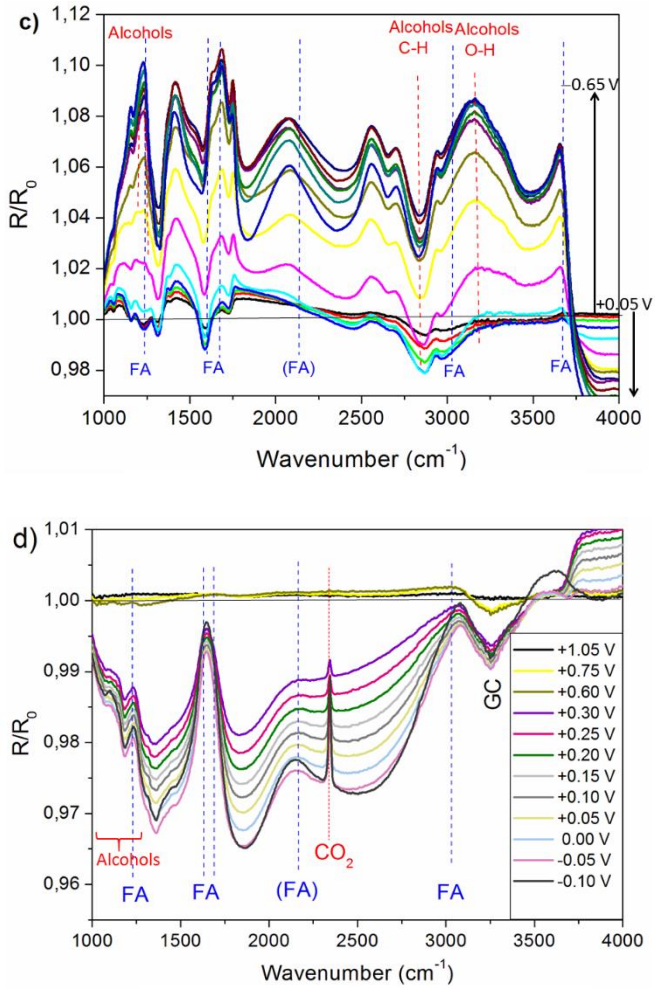

Figure 3: a) Linear sweep voltammetry at a scan rate of 1 mV·s^{-1}, 0.1 mol·L^{-1} Na_2SO_4, N_2 saturated (black curve), CO_2 saturated (red), and containing 4.3 mol·L^{-1} FA (blue) using a PTFE-free In_2O_3 cathode, b) Relative reflectance in IR spectroelectrochemistry of 4.3 mol·L^{-1} FA with a PTFE-free In_2O_3 cathode as the working electrode in the potential range of +1.0 V (baseline at R/R_0 = 1.00) and to –0.4 V decreasing in 100 mV intervals. The red arrow indicates increasing formation of CO_2, the blue arrows indicate the decreasing concentrations of FA. c) Relative IR reflectance observed with 4.3 mol·L^{-1} formic acid with PTFE-free In_2O_3 cathode as the working electrode in the potential range of 0.05 V (baseline at R/R_0 = 1.00) to –0.65 V decreasing in 50 mV intervals. d) Relative reflectance obtained with CO_2 saturated 0.1 mol·L^{-1} Na_2SO_4 with 0.15 wt% PTFE-containing In_2O_3 working electrode at potentials of +1.05 V (baseline at R/R_0 = 1.00) to –0.10. All potentials are relative to RHE.

b) Oxidation of formic acid

The data of IR spectroelectrochemical experiments are shown in Figures 3b to 3d. Aqueous formic acid is thermodynamically unstable against decay into H_2 and CO_2 as well as into H_2O and CO, although these reactions are both highly activated.[19] Figure 3b largely represents the oxidative regime where FA is consumed and CO_2 is formed. This simple reaction permits an unequivocal assignment of bands. In agreement with expectation, we find the unmistakable asymmetric stretching mode of "free" CO_2 at 2342 cm^{-1} growing with time. The CO_2 bending mode is expected at 667 cm^{-1}, well outside the observation window. An expansion of the spectra in the proximity of the asymmetric CO_2 stretching mode reveals a slightly more complicated picture (Figure ESI 1) with two side bands appearing, suggesting that two further surface sites become accessible for CO_2 adsorption at more negative potentials. The 2336 cm^{-1} feature could even represent linearly bound CO_2. [20]

The vibrational spectra of formic acid are quite variable and depend on the syn and anti-conformations of the acid group, the formation of dimers through hydrogen bonding, general solvation and intermolecular hydrogen bonding in aqueous environments, partial deprotonation, fast proton exchange, and even hydrophobic interactions.[21,22] Neat formic acid shows three dominant bands at 3125 cm^{-1}, 1724 cm^{-1} and 1190 cm^{-1}, a medium intensity band at 1351 cm^{-1}, a weak band at 1063 cm^{-1}, and an incompletely resolved multiplet in the C–H stretching regime (2941, 2700 and 2564 cm^{-1}) indicating splitting due to dimer formation (Table ESI 1). For comparison, calculated values for the corresponding vibrational modes of gas phase monomeric FA are 3570 cm^{-1}, 2943 cm^{-1}, 1770 cm^{-1}, 1387 cm^{-1}, 1229 cm^{-1}, and 1033 cm^{-1} in fair agreement with the experimental values in the liquid.[23] In the Aldrich catalogue these bands show near 3125 cm^{-1}, 2800 cm^{-1}, 1724 cm^{-1}, 1351 cm^{-1}, 1190 cm^{-1}, and 1064 cm^{-1}. Adsorption on a catalytic surface complicates the situation further.[24]

In the present case (Figure 3b), consumption of FA leads to concerted decreasing reflection (R/R_0>1) of the main vibrational modes in the observation window: a double band near 1667/1589 cm^{-1} assigned to C=O stretching of formic acid and formate, respectively, possibly containing a contribution from water bending as well, and the band at 1225 cm^{-1} corresponding to C–O stretching. Two more main bands are assigned to the C–H and O–H stretching modes at 3037 cm^{-1} and 3670 cm^{-1}, respectively. The variation of intensities of these bands as a function of applied potential are well correlated (see Figure ESI 2a), suggesting that they belong to the same species, and there seems to be little or no interference of water or broad ice bands (Figure ESI 2b). Another dominant band at 2120 cm^{-1} is also correlated to FA but occurs at an unusually high position, so the assignment is displayed in parentheses. The observed differences in wavenumber values may be ascribed to the interaction with the catalyst and the presence of the aqueous environment. In Figure 3b, the positions of weak bands arising between 1000 and 1250 cm^{-1} are also indicated as these might correspond to the formation of alcohols (reference spectra of alcohols in 0.1 mol·L^{-1} Na_2SO_4 showing the characteristic low wavenumber bands are provided in Fig. ESI 3, numerical values in Table ESI 1).

c) Reduction of formic acid

Figure 3c shows highly structured spectra in the reductive regime starting from open circuit potential (open circuit potential = 0.05 V)

down to −0.65 V, revealing a rich chemistry that is difficult to interpret. The nominal positions of FA bands based on Figure 3b are indicated by dashed lines. The spectra, although heavily overlapped, are roughly compatible with the disappearance of FA, within the dominance of $R/R_0>1$. As expected, there is no indication of CO_2. Superimposed, there are highly structured indications of product formation ($R/R_0<0$), possibly compatible with alcohols or hydrocarbons, in particular also the relatively strong feature around 2800 cm^{-1} that is typical for C–H stretching bands but contradicted by the O–H stretching regime which is dominated by a disappearing feature with $R/R_0>1$.

d) Reduction of aqueous carbon dioxide

Figure 3d was measured in 0.1 $mol·L^{-1}$ Na_2SO_4 saturated with CO_2 in the absence of FA, but at potentials comparable to those in Figure 3b. Furthermore, PTFE was added to the cathode catalyst. The obvious difference is that while 3b spectra are dominated by the disappearance of FA and formation of CO_2, the spectra of 3d reveal mainly the formation of intermediates and products, seen as a broad, structured background superimposed by the disappearance of CO_2. In agreement with expectation, the CO_2 band changes in the positive direction, demonstrating that CO_2 is consumed as the applied potential trends more negative. Identification of the intermediates and products is somewhat speculative, but small features in the low wavenumber region are compatible with alcohols as products. The positions of the FA bands from Figure 3b are again indicated, and it is quite clear that there is little or no change in reflectivity at these positions, revealing no evidence of intermediate FA formation. The strong band with potential-dependent intensity at 3261 cm^{-1} is compatible with the O–H stretching mode on the surface of glassy carbon (GC).[25] Alternatively, oxidation-state-dependent chemisorbed hydrogen on the In_2O_3 catalyst (see Scheme 1 below) may give rise to similar features. However, the key information of this experiment is that the catalyst works not only with FA but also efficiently with dissolved CO_2, despite its low solubility, as concluded already from the LSV experiments of Figure 3a.

Comparison of the spectra of formic acid reduction (Figure 3c) and aqueous CO_2 reduction (Figure 3d) reveals important differences in the diminishing reflection peaks ($R/R_0<1$), revealing that the products and intermediates of the two reactions are quite different. In agreement with the above finding that CO_2 reacts faster than formic acid without leading to a pile-up of FA concentration in Figure 3d we conclude that on the present catalyst CO_2 bypasses formic acid as an intermediate. Comparison with literature work that reports the formation of formate [11-13] demonstrates that slight differences in the preparation of the indium catalyst have important consequences on the product distribution.

FA electrolysis and efficiency aspects

a) The effect of added PTFE to the cathode catalyst on current densities

Figure 4a shows the results of LSV experiments of FA in a polymer electrolyte membrane electrolyser cell. The standard TaC-supported IrO_2 water splitting anode catalyst was coated on Nafion® 117, layered by a titanium mesh that served as the gas diffusion layer and capped by another titanium mesh which served as the current collector. This is in analogy to the work of Polonský *et al.*[26] except that their experiments were conducted at elevated temperatures, ranging from 90 °C, to 130 °C, while the present study was performed between 22 °C and 24 °C. The cathode consisted of In_2O_3 with added PTFE, coated on carbon paper which functioned as a gas diffusion electrode, while titanium mesh served as current collector. The catholyte was 4.3 $mol·L^{-1}$ aqueous formic acid. It is obvious from Figure 4a that the addition of PTFE (red and blue traces) increases the current density at an applied cell voltage of 2.4 V by a factor of ca. 30. The slope of a linear asymptote of the high voltage branch of early cycles (i.e. before depletion near the electrode sets in and causes additional transport resistance) of LSV curves gives the Ohmic resistance of the membrane-electrode assembly. Its extrapolation to zero current provides the onset potential in the absence of Ohmic contributions, which is typically ca. 2.2 V for fresh samples without PTFE in the catalyst (black curve), but 1.8 V with 0.30 wt% admixed PTFE (blue and red curves in Figure 4a). The main effect of PTFE is reducing the area resistivity from 155 $Ω·cm^2$ to 10 $Ω·cm^2$ (derived from the LSV slope in Figure 4a) at a fraction of 0.30 wt%. At a current density of 70 $mA·cm^{-2}$, a 10 $Ω·cm^2$ resistivity corresponds to a potential drop of 700 mV, equivalent to an energy loss of 68 kJ per mol electrons. Secondly, the addition of PTFE reduces the activation polarization of the electrode reaction by about 400 mV, revealing a direct interaction of PTFE with the catalyst surface. The standard free enthalpy of reaction ($\Delta G°$) of formic acid amounts to +432.1 kJ mol^{-1} ($|\Delta E°| = \Delta G°/nF$ = 1.12 V, n is the number of transferred electrons) for the formation of methanol, +785.0 $kJ·mol^{-1}$ (1.02 V) for ethanol, and +1141.0 $kJ·mol^{-1}$ (0.99 V) for iso-propanol. The offset of the effective experimental onset potential of 1.8 V from the absolute $\Delta E°$ values translates into effective electrochemical activation energies per electron of 66 $kJ·mol^{-1}$ for methanol, 75 $kJ·mol^{-1}$ for ethanol, and 78 $kJ·mol^{-1}$ for iso-propanol.

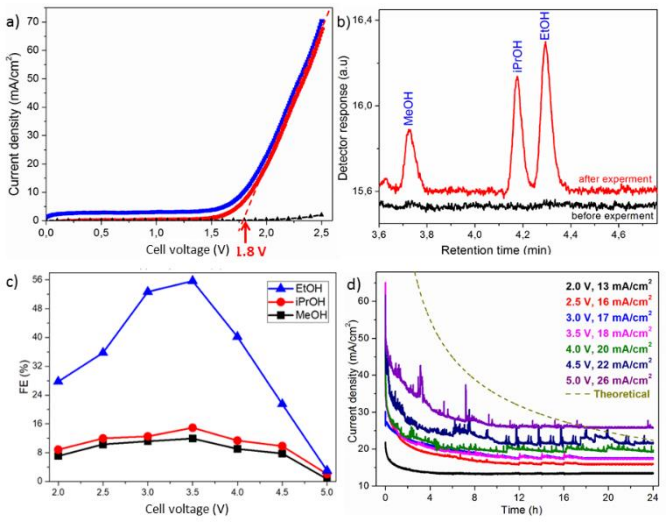

Figure 4: Co-electrolysis of water at a conventional water electrolysis anode and aqueous FA (4.3 mol·L^{-1}) on In_2O_3 at the cathode: a) Linear sweep voltammetry (scan rate 10 mV·s^{-1}). Black: plain In_2O_3 cathode catalyst, blue and red: cycle 1 and 5, respectively, of In_2O_3 intermixed with 0.30 wt% PTFE. The arrow indicates the onset potential at 1.8 V. b) GC analysis of aqueous product phase from water-FA co-electrolysis (red curve from panel (a) at 2.4 V applied cell voltage). c) FE as a function of applied cell voltage (cathode: In_2O_3/0.30 wt% PTFE). d) Chronoamperometric curves at different applied cell voltage saturate at the current densities given in the inset. The theoretical curve gives the Cottrell behavior for diffusion-controlled reactions. (Two-column figure)

We refrain from a Tafel analysis that in principle can provide mechanistic information about the rate-determining step, for example, whether it involves a single or double electron transfer. However, the entire Figure 4 was measured in a two-electrode setup and is therefore given as a function of the cell voltage. This involves the water oxidation reaction at the anode and the formation of a mixture of methanol, ethanol, isopropanol and hydrogen (see below), and it can be complicated further by the extent of coverage of the electrodes by adsorbed reactants. [27] Tafel plots of the same experiment obtained for the cathode reaction with a three-electron setup against a reference electrode are shown in Figure ESI 6. They reflect the enormously enhanced current densities resulting from addition of PTFE to the cathode catalyst that is already obvious from the LSV curves. The plots are of good linearity in the relevant range, leaving no possibility to discriminate between different products.The rate determining step of the multi-electron transfer in the formation of the three alcohols (but quite likely not of hydrogen) may be the same. The Tafel slopes are significantly enhanced over the value of 120 mV/dec that is normally expected for single electron transfer, or of 60 mV/dec for double electron transfer.

b) Product analysis and Faraday efficiency

Figure 4b displays the typical GC analysis of the products collected in liquid water after 24 h electrolysis. It shows three clear peaks, revealing the formation of methanol, ethanol and iso-propanol. No other products were detected in the liquid catholyte. The alcohol GC peak areas were calibrated using standard samples (see ESI Figure 4). Figure 4c shows the FE of the liquid products of FA reduction as a function of the applied cell voltage. The maximum FE is observed at a cell voltage of 3.5 V, with 11.9%, 55.7%, and 14.9%, for methanol, ethanol and iso-propanol, respectively, corresponding to an impressive total FE of 82.5%. These numbers are proportional to the chromatographically determined amounts of product and represent the percentage of electrochemically transferred electrons which arrive in the product. They simply reflect the formation of product from one mole of formic acid, which requires transfer of n = 4 electrons for methanol, 8 for ethanol, and 12 for iso-propanol. The remaining 17.5% of the electrons relate to gas phase products, mainly hydrogen, since no other gas phase product molecules like CO, CH_4 or ethene were detected. Such a high yield of C_2 and C_3 alcohols requires that intermediates of two or three molecules derived from formic acid must recombine efficiently, which implies that they are either formed in close proximity and/or that they are mobile on the catalyst surface. It is noted that the bixbyite structure of In_2O_3 contains regular structural oxygen vacancies,[28] which can conceivably bind both, HCOOH or CO_2, via their carboxyl or carbonyl oxygen (Figure ESI 5).

Thermodynamically, iso-propanol is the most and methanol the least favoured product. The experimental product distribution is roughly constant over the range of applied voltages, but it does not follow the product stability, which demonstrates kinetic control of the electrocatalytic reaction.

All three alcohols are formed with no other products present in the aqueous phase, independent of the addition of PTFE to the cathode catalyst. The relative yields of methanol and ethanol are independent of the amount of added PTFE, however, the relative yield of iso-propanol is enhanced by PTFE (see Figure ESI 7). On the other hand, the FE of ethanol depends much ore on the magnitude of the cell voltage, while the FE of methanol and iso-propanol are nearly the same and less variable. The origin of variations of these relative product distributions is not clear at present.

The space-time-yield of the FA reduction reaction at 3.5 V, 20 mA·cm^{-2} and room temperature is calculated, based on Figure 4c, to be 0.43 g as a sum of the three alcohols per h and per g In_2O_3. This is only a factor of 2.2 less than the most recent value reported for CO_2 conversion by Frei *et al*. obtained using heterogeneous thermal catalysis with specifically engineered Pd-promoted In_2O_3 at 553 K and a hydrogen pressure of 50 MPa, and it is about double of the value for plain In_2O_3.[8] Increasing the steady-state current density with an active catholyte flow to 70 mA·cm^{-2} should increase the space-time yield by a factor 3.5 to 1.5 g per hour and gram catalyst. It should be noted that the values are not exactly comparable since the present experiment uses water and FA as reactants whereas the literature experiment starts with H_2 and CO_2.

c) Diffusion limitation

The FE decreases with applied cell voltage beyond its maximum at 3.5 V. This is understood based on the chronoamperometric curves displayed in Figure 4d. The curves start at current density values near 80 mA·cm^{-2} but drop rapidly, reaching potential dependent plateau values beyond ca. 12 h. The Cottrell equation

$$i/area = nFc_0\sqrt{D/\pi t} \qquad (1)$$

describes the time dependence of the current density of a convection-free, diffusion-controlled (non-activated) reaction near a planar electrode, with $i/area$ the current density in A·cm^{-2}, n the number of electrons needed to reduce FA, F the Faraday constant, c_0 the initial concentration of the reactant, D the diffusion coefficient in $cm^2 \cdot s^{-1}$, and t the time in s.[29] The theoretical curve according to eqn. (1) using n= 8 for ethanol and D = 14.1×10^{-6} $cm^2 \cdot s^{-1}$ for FA is

plotted in Figure 4d and shown to reproduce qualitatively the experimental behaviour, confirming that a diffusion layer builds up and leads to reactant depletion near the electrode surface. Lower current densities at short times and the offsets with increasing potential are because the electrode reaction is activated (eqn. 1 does not contain the applied cell voltage). Higher current densities at long times indicate a reduction of the diffusion gradient, for example by the effect of thermal convection, enhanced by bubble formation of gaseous products as indicated by the spikes at higher current densities. Depletion in the stationary FA solution near the cathode will likely lead to more H_2 formation, since the organic reactant is not available, which is in agreement with the decrease of the FE beyond 3.5 V (Figure 4c). In addition, beyond 3.5 V cell voltage, the cathode potential reaches the dominant HER domain (Figure 2b, wave c3). The amplification of this competing reaction has been observed previously.[30] The slow decrease of the current density beyond 10 h demonstrates the excellent stability of the electrodes. In fact, at 3.5 V, a decrease of 16% over 24 h is related to bulk reactant depletion due to consumed FA, the rest to electrode stability.

d) Energy efficiency

The electrical work spent per transferred electron amounts to ηF, where η is the cell polarisation. It contains mainly three contributions; the activation energy of the two electrode reactions, i.e. the oxygen evolution at the anode and the formic acid, CO_2 or proton reduction at the cathode; the Ohmic resistance of formic acid transport in solution, and the Ohmic heat dissipated in the membrane-electrode unit.

The energy efficiency (EE) decreases with increasing cell voltage since the offset beyond the Nernst potential $\Delta E°$ represents a loss due to non-equilibriuum. It can be estimated from

$$EE = FE \times \Delta E° / U \qquad (2)$$

where U is the applied cell voltage. These values, tabulated in Table ESI 2, are approximate since the local conditions at the electrode surfaces do not exactly correspond to standard states assumed in $\Delta E°$. They decrease only slowly at low cell potentials since the effect of the offset from equilibrium is partly compensated by the increasing FE.

Today, most CO_2 electroreduction experiments are conducted using liquid catholyte and normally an H-cell geometry with a large anode-cathode separation as used historically for equilibrium measurements in the limit of zero current densities. Measured current densities are therefore often at best a few mA·cm^{-2}. Industrial applications, however, require current densities on the order of several hundred mA cm^{-2} to be economical.[31] Typical current densities of fuel cells and water electrolyzers reach one to several A·cm^{-2}, which is made possible due to the low membrane electrolyte separator of a thickness of ca. 180 µm to reduce the Ohmic resistance. Moreover, transport is more efficient in the gas phase than in solution by several orders of magnitude, and suitable hydrophobization of the gas diffusion layer in contact with the electrocatalyst prevents flooding of the electrode with concomittant reduction of transport coefficients of gaseous reactants and products in the pores. In the present case, the diffusion coefficient of CO_2 at 1 bar pressure will be D = 0.16 cm^2·s^{-1}, four orders of magnitude larger than for aqueous formic acid. It enters as the square root in eqn. (1), leaving a gain of two orders of magnitude in transport efficiency, which is counterbalanced by the gas phase concentration at 1 bar, compared to 4.3 mol·L^{-1} FA. High currents can still be obtained since gas flow and higher convection prevent the build-up of a depletion layer, as is demonstrated by current densities of several A·cm^{-2} in PEM fuel cells.

In agreement with the cyclic voltammetry, spectroelectrochemistry and electrolysis experiments, one may propose a plausible mechanism for FA reduction to methanol on the In_2O_3 cathode. Firstly, In_2O_3 is electrochemically reduced to In^0.[15] At the same potential, an In-H$^*_{ads}$ surface species is formed by a 1 electron reduction of H^+. This active species can then transfer 2 electrons and a proton to FA to form the In^I species observed in cyclic voltammetry and the intermediate methanediol, the hydrated form of formaldehyde. In^I is readily reduced to In^0, which closes the catalytic cycle. The methanediol close to the surface can then undergo an additional reduction induced by the In-H$^*_{ads}$ surface species resulting in methanol. Then, higher alcohols may be formed through the same stepwise reduction pattern involving the different intermediate species formed.

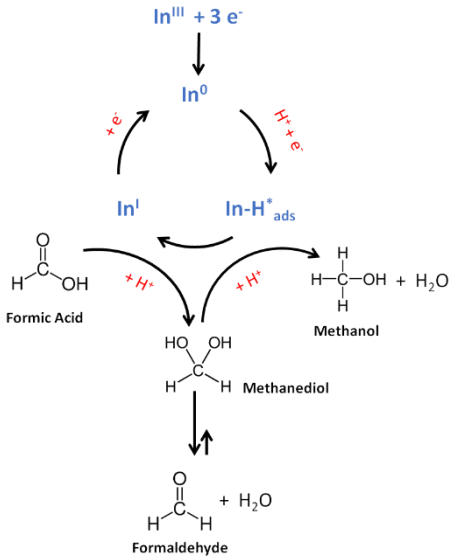

Scheme 1: Proposed mechanism for FA reduction to methanol

Conclusions

It is shown here that nanosized indium oxide is not only highly active as a thermal heterogeneous catalyst for the hydrogenation of CO_2 with 100% selectivity to methanol [6] but also a very active electrocatalyst at room temperature, with water as a hydrogen source. In this latter case, a mixture of the three alcohols methanol,

ethanol and iso-propanol is formed with up to 82.5% FE, starting from FA, the remaining FE relating to H_2. The addition of a small amount of PTFE to the catalyst leads to an improvement of the current density by a factor of ca. 30 at an applied cell voltage of 2.4 V. This reduces the onset potential of the electroreduction by ca. 0.4 V and the Ohmic resistance of the cell by a factor of 15, indicating that both the electrode activation energy and the transport resistance in the porous structure are reduced. The latter is likely due to the increased hydrophobicity in the porous catalyst layer. At a 4.3 $mol \cdot L^{-1}$ FA concentration and in the absence of stirring, the steady-state current density is limited to ca. 20 $mA \cdot cm^{-2}$. Since the initial current density amounts to at least 70 $mA \cdot cm^{-2}$, it is concluded that the limitation is due to formic acid transport across the diffusion layer near the catalyst surface. It is expected that an active flow of the catholyte that eliminates the diffusion layer will increase the steady-state current density towards 70 $mA \cdot cm^{-2}$ at the same cell voltage and without an increase of hydrogen formation.

Kim et al. [14] did not observe any ethanol or iso-propanol, confirming that the details of the preparation of the In_2O_3 catalyst are crucial.

Minimisation of the Ohmic resistance by reducing the distance between cathode and anode to less than 100 μm suggests the use of a polyelectrolyte membrane configuration. Furthermore, for high current densities, it is recommended to apply CO_2 in the form of a gas instead of a solution due to the much higher transport coefficients in the gas phase and the avoidance of its solubility limit. Further work in this direction looks highly promising for industrial applications.

While the main focus of the present work is on the efficient reduction of aqueous FA to methanol, ethanol and iso-propanol, preliminary experiments showed that aqueous CO_2 solutions react even more efficiently than FA, but no product determination is available at this point. Further work will have to clarify the mechanistic implications of these findings.

Conflicts of interest

There are no conflicts to declare.

Acknowledgements

We thank the University of Pretoria for financial support via the IRT Energy and the South African NRF for support via the SSAJRP Program (UID 87401) and via the PROTEA Program (Nr. 42442PF) together with France (NAF 8542 Z). K. A. Adegoke thanks for his NRF TWAS fellowship for the Doctoral Scholarship Award ((Nr. 42442PF/NRF UID: 105453 & Reference: SFH160618172220, and MND190603441389 & Unique Grant No: 121108) and UP Postgraduate Doctoral Research bursary award. The PhD fellowship to P. Rayess from the ANR (EClock project) is gratefully acknowledged. We thank Prof. Plietker from the University of Stuttgart on a donation of a motherboard for our GC instrument.

References

1. https://ec.europa.eu/jrc/en/jec/renewable-energy-recast-2030-red-ii (Downloaded 26.08.2019).
2. K. P. Kuhl, R. Cave, D. N. Abram and T. F. Jaramillo, New insights into the electrochemical reduction of carbon dioxide on metallic copper. *Energy Environ. Sci.*, 2012, **5**, 7050-7059.
3. D. Kim, C. S. Kley, Y. Li, R. Yang, Copper nanoparticles for selective electroreduction of CO_2 to C_2-C_3 products. *PNAS*, 2017, **114,** 10560-10565.
4. Y. Song, R. Peng, D. K. Hensley, V. Bonnesen, L. Liang, Z. Wu, H. M. Meyer, M. Chi, C. Ma, B. G. Sumpter and A. J. Rondinone, High-Selectivity Electrochemical Conversion of CO_2 to Ethanol using a Copper Nanoparticle/N-Doped Graphene. *Chemistry Select.* 2016, **1**, 6055-6061.
5. K. U. D. Calvinho, A. B. Laursen, K. M. K. Yap, T. A. Goetjen, S. Hwang, N. Murali, B. Mejia-Sosa, A. Lubarski, K. M. Teeluck, E. S. Hall, E. Garfunkel, M. Greenblatt and C. Dismukes, Selective CO_2 reduction to C_3 and C_4 oxyhydrocarbons on nickel phosphides at overpotentials as low as 10 mV. *Energy Environ. Sci.*, 2018, **11**, 2550-2559.
6. O. Martin, A. J. Martín, C. Mondelli, S. Mitchell, T. F. Segawa, R. Hauert, C. Drouilly, D. Curulla-Ferré and J. Pérez-Ramiréz, Indium oxide as a superior catalyst for methanol synthesis by CO_2 hydrogenation. *Angew. Chem. Int. Ed*., 2016 **55**, 6261–6265.
7. A. García-Trenco, A. Regoutz, E. R. White, D. J. Payne, M. S.P. Shaffer, and C. K. Williams, *Appl. Cat. B, Environmental*, 2018, **220**, 9-18.
8. M. S. Frei, C. Mondelli, R. García-Muelas, K. S. Kley, B. Puértolas, N. Lopéz, O. V. Safonova, J. A. Stewart, D. Curulla Ferré and J. Pérez-Ramirez, J., Atomic-scale engineering of indium oxide promotion by palladium for methanol production via CO_2 hydrogenation. *Nature Commun.* (2019) 10:3377.
9. O. Bierwagen, Indium oxide - a transparent, wide-band gap semiconductor for (opto)electronic applications. *Semicond. Sci. Tech.* 2015, **30**, 024001.
10. B. Zhang, N. N. Zhang, J. F. Chen, Y. Hou, S. Yang, J. W. Guo, X. H. Yang, J. H. Zhang, H. F. Wang, P. Hu, H. J. Zhao and H. G. Yang, Turning Indium Oxide into a Superior Electrocatalyst: Deterministic Heteroatoms. *Sci. Rep.*, 2013, **3**, 3109.
11. Z. M. Detweiler, J. L. White, S. L. Bernasek and A.B. Bocarsly, Anodized Indium Metal Electrodes for Enhanced Carbon Dioxide Reduction in Aqueous Electrolyte, *Langmuir*, 2014, **30**, 7593-7600.
12. J. L. White and A. B. Bocarsly, Enhanced Carbon Dioxide Reduction Activity on Indium-Based Nanoparticles. *J. Electrochem. Soc.*, 2016, **163,** H410-H416.
13. K. Mou, Z. Chen, S. Yao and L. Liu, Enhanced electrochemical reduction of carbon dioxide to formate with in-situ grown indium-based catalysts in an aqueous electrolyte, *Electrochim Acta*, 2018, **289**, 65-71
14. M.-G. Kim, J. Jeong, Y. Choi, J. Park, E. Park, C.-H. Cheon, N.-K. Kim, B. Koun Min and W. Kim, Synthesis of V-doped In_2O_3 Nanocrystals via Digestive-Ripening Process and Their Electrocatalytic Properties in CO_2 Reduction Reaction, *ACS Appl. Mat. & Interfaces*, 2020, **12**, 11890 – 11897.

15. C. I. Shaughnessy, D. T. Jantz and K. C. Leonhard, Selective electrochemical CO_2 reduction to CO using in situ reduced In_2O_3 nanocatalysts. *J. Mat. Chem. A*, 2017, **5**, 22743-22749.
16. F. P. García de Arquer, C.-T. Dinh, A. Ozden, J. Wicks, C. McCallum, A. R. Kirmani, D.-H. Nam, C. Gabardo, A. Seifitokaldani, X. Wang, Y. C. Li, F. Li, J. Edwards, L. J. Richter, S. J. Thorpe, D. Sinton, E. H. Sargent, CO_2 electrolysis to multicarbon products at activities greater than 1 A cm^{-2}, *Science*, 2020, **367**, 661-666.
17. E. Laviron, General expression of the linear potential sweep voltammogram in the case of diffusionless electrochemical systems. *J. Electroanal. Chem. Interfacial Electrochem.* 1979, **101**, 19-28.
18. L. Wang, T. Yan, R. Song, W. Sun, Y. Dong, J. Guo, Z. Zhang, X. Wang, G. A. Ozin, Room-Temperature activation of H_2 by a surface frustrated Lewis pair. *Angew. Chem. Int. Ed.* 2019, **58,** 9501-9505.
19. Roduner, E., Understanding Catalysis, *Chem. Soc. Rev.* **2014, 43**, 8226-8239.
20. Szanyi, J, Kwak, J. H., Dissecting the steps of CO_2 reduction: 1. The interaction of CO and CO_2 with γ-Al_2O_3: an in situ FTIR study. *Phys. Chem. Chem. Phys.,* 2014, **16**, 15117-15125.
21. G. Giubertoni, O. O. Sofronov and H. J. Bakker, Observation of distinct carboxylic acid conformers in aqueous solution. *J. Phys. Chem. Lett.*, 2019, **10**, 3217-3222.
22. J. Chen, C. L. Brooks and H. A. Scheraga, Revisiting the Carboxylic Acid Dimers in Aqueous Solution: Interplay of Hydrogen Bonding, Hydrophobic Interactions, and Entropy. *J. Phys. Chem.* B, 2008, **112**, 242-249.
23. H. Susi and J. R. Scherrer, The normal vibrations of formic acid and methyl formate. *Spectrochim. Acta*, 1969, **25A**, 1243-1263.
24. Y. Zhang, X. Chen, B. Zheng, X. Guo, Y. Pan, H. Chen, H. Li, S. Min, C. Guan, K-W. Huang and J. Zheng, Structural analysis of transient reaction intermediate in formic acid dehydrogenation catalysis using two-dimensional IR spectroscopy. *PNAS*, 2018, **115**, 12395-12400.
25. W. Koutek, A. Conradi, Ch. Fabjan, G. Bauer, G., In situ FTIR spectroscopy of the Zn – Br battery bromine storage complex at glassy carbon electrode, *Electrochim. Acta,* 2001, **47**, 815-823.
26. J. Polonský, P. Mazúr, M. Paidar, E. Christensen and K. Bouzek, Performance of a PEM water electrolyser using a TaC-supported iridium oxide electrocatalyst. *Int. J. Hydrogen Energy*. 2014, **39**, 3072–3078.
27. T. Shinagawa, A. T. Garcia-Esparza, K. Takanabe, Insight from Tafel slopes from a microkinetic analysis of aqueous electrocatalysis for energy conversion. *Scientific Reports*, 2015, **15**, 13801.
28. D. B. Buchholz, Q. Ma, D. Alducin, A. Ponce, M. Jose-Jacaman, R. Khanal, J. E. Medvedeva and R. P. H. Chang, The structure and properties of amorphous indium oxide. *Chem. Mater.*, 2014, **26**, 5401-5411.
29. F. G. Cottrell, Der Reststrom bei galvanischer Polarisation, betrachtet als Diffusionsproblem, *Z. Phys. Chem*. 1903, **42**, 385-431.
30. I. Kotoulas, A. Schizodimou and G. Kyriacou, Electrochemical reduction of formic acid on a copper-tin-lead cathode, *Open Electrocem. J.*, 2013, **5**, 8-12.
31. T. Burdyny and W. A. Smith, CO_2 reduction on gas-diffusion electrodes and why catalytic performance must be assessed at commercially relevant conditions. *Energy Environ. Sci.*, 2019. **12**, 1442-1453.

Graphical abstract